

Construction of the Free Energy Landscape of Peptide Aggregation from Molecular Dynamics Simulations

Laura Riccardi,[†] Phuong H. Nguyen,[‡] and Gerhard Stock^{*,†}

[†]Biomolecular Dynamics, Institute of Physics, Albert Ludwigs University, 79104 Freiburg, Germany

[‡]Laboratoire de Biochimie Theorique - UPR 9080, Institut de Biologie Physico-Chimique, 13, rue Pierre et Marie Curie, F-75005 Paris, France

S Supporting Information

ABSTRACT: To describe the structure and dynamics of oligomers during peptide aggregation, a method is proposed that considers both the intramolecular and intermolecular structures of the multimolecule system and correctly accounts for its degeneracy. The approach is based on the “by-parts” strategy, which partitions a complex molecular system into parts, determines the metastable conformational states of each part, and describes the overall conformational state of the system in terms of a product basis of the states of the parts. Starting from a molecular dynamics simulation of n molecules, the method consists of three steps: (i) characterization of the *intramolecular* structure, that is, of the conformational states of a single molecule in the presence of the other molecules (e.g., β -strand or random coil); (ii) characterization of the *intermolecular* structure through the identification of all occurring aggregate states of the peptides (dimers, trimers, etc.); and (iii) construction of the *overall* conformational states of the system in terms of a product basis of the n “single-molecule” states and the aggregate states. Considering the Alzheimer β -amyloid peptide fragment $A\beta_{16-22}$ as a first application, about 700 overall conformational states of the trimer $(A\beta_{16-22})_3$ were constructed from all-atom molecular dynamics simulation in explicit water. Based on these states, a transition network reflecting the free energy landscape of the aggregation process can be constructed that facilitates the identification of the aggregation pathways.

1. INTRODUCTION

A broad range of diseases are associated with the conversion of polypeptide chains from their normally soluble form to insoluble fibrillar aggregates.^{1,2} These disorders include neurodegenerative conditions, such as Alzheimer’s disease, Parkinson’s disease, and the spongiform encephalopathies. They also include both systemic and localized amyloidoses.^{3,4} The amyloid structure is defined in terms of experimental descriptors. From electron microscopy the amyloid fibrils appear straight and unbranched.⁵ X-ray fiber diffraction experiments indicate a characteristic cross-structure in which the polypeptides form strands oriented perpendicular to the long axis of propagation of the fibril.^{3,5} Moreover, this global structure is common even if the proteins involved in amyloid diseases lack sequence homologies and do not have a common native three-dimensional fold.⁶ It has been suggested based on experiments that amyloid formation can be achieved by almost all polypeptide chains under appropriate conditions.^{3,6} The idea of an intrinsic property of forming amyloid aggregates and the observation of a common structure indicate that the aggregate is stabilized by intermolecular interactions common to all proteins, such as backbone hydrogen bonding or hydrophobic interactions, rather than more specific side-chain interactions.^{1,6} Although there might be a generic mechanism for the aggregation, it is likely that there are several distinct scenarios for the aggregation to take place.⁷

Because of the relation between pathogenesis of known diseases and aggregation, as well as the complexity of amyloid fibril formation, numerous experimental^{3–8} and computational^{9–18} studies have been performed, leading to a micro-

scopic picture of the oligomerization process. The final aim is to extract unifying principles governing peptide and protein aggregation. The characterization of the molecular details in the cascade of structural transitions is fundamental in understanding amyloid formation.¹⁹ Fluctuations of the monomer conformations involved in the initial steps of protein aggregation are believed to lead to oligomerization and fibril assembly.²⁰ Moreover, the oligomers preceding the formation of well-defined fibrils seem to play a critical role in the pathogenesis of the aggregation diseases. Therefore, the identification and characterization of such species is of particular interest.⁴

One of the most studied pathogenic peptides is the Alzheimer β -amyloid peptide ($A\beta$). Its fragment $A\beta_{16-22}$ with sequence Lys-Leu-Val-Phe-Phe-Ala-Glu corresponds to residues 16–22 of the full-length (40-amino-acid) peptide.²¹ It appears to be a perfect model system, as it is among the shortest fragments of the full β -amyloid peptide that is able to form fibrils. Moreover, residues 17–21 constitute a hydrophobic core that is likely to be essential for fibrillization of full-length β -amyloid peptides.²¹ The system has been investigated experimentally by, for example, solid-state ¹³C NMR spectroscopy, electron microscopy, and X-ray diffraction,²¹ as well as computationally by Monte Carlo simulations²² and molecular dynamics (MD) simulations.^{23–30}

As the oligomerization mechanism appears to be complex and system-specific,¹⁹ the identification of unique parameters

Received: December 20, 2011

Published: February 28, 2012

that help to unravel the complexity is challenging. With this end in mind, several order parameters such as the radius of gyration,^{31,32} root-mean-square distance,¹² end-to-end distance,³¹ fraction of native contacts,³¹ and orientational order parameter P_2 have been employed.⁹ The task is further complicated by the fact that, apart from the intermolecular degrees of freedom, intramolecular degrees of freedom of the various monomers need to be considered. With this end in mind, de Groot and co-workers recently analyzed peptide oligomerization in terms of dimer conformations.¹⁸ Employing extensive MD simulations of short steric zipper peptides, the various aggregate states that occurred during the oligomerization process were mapped onto a space of reduced dimensionality.

As an alternative approach, Nguyen et al.²⁹ employed dihedral-angle principal component analysis (dPCA; see section 2) to study the dynamics of formation of the $(A\beta_{16-22})_n$ ($n = 4-6$) oligomer. Figure 1A shows the resulting free energy

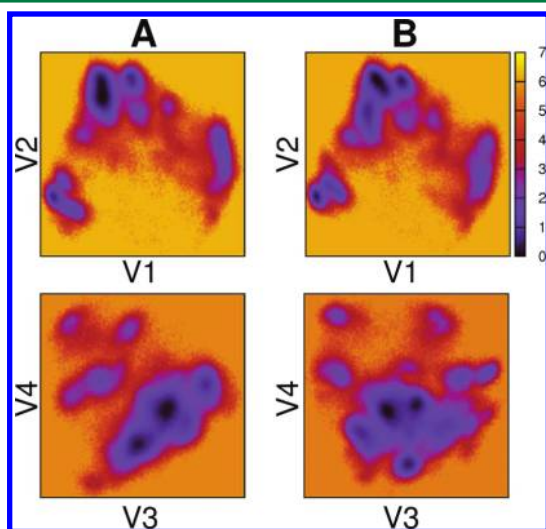


Figure 1. Free energy landscape (in units of $k_B T$) of the trimer $(A\beta_{16-22})_3$, shown as a function of the principal components (V_1, V_2) (top) and (V_3, V_4) (bottom). (A) Simple dPCA of all φ and ψ dihedral angles of the trimer and (B) dPCA that also includes an angle for each pair of monomers that accounts for their relative orientation.

surface for the trimer $(A\beta_{16-22})_3$ as a function of the first few principal components. The energy landscape exhibits several clearly distinguishable minima, corresponding to metastable conformational states that are separated by small free energy barriers. However, a closer analysis of the underlying molecular structures reveals that the minima in Figure 1A correspond not to unique global conformations of the oligomer, but rather to a superposition of different ones. This might be due to the fact that dPCA uses only internal coordinates (i.e., the φ and ψ dihedral angles of the peptide backbone) but does not contain any information about the relative positions and orientations of the different peptides. To account as well for the relative orientations of the various molecules, it has been suggested that the angle between the corresponding vectors connecting the C_α atoms of 1Lys and 7Glu be included in dPCA.³³ Surprisingly, however, this procedure is found to hardly improve the structural resolution of the free energy landscape of $(A\beta_{16-22})_3$; see Figure 1B. Similar results were obtained when we tried to combine dPCA with the orientational order parameter P_2 (data not shown).

A more thorough analysis shows that the above findings are related to the fact that, in our analysis, we treated the various molecules as *distinguishable* entities. However, each molecule is an exact copy of the others. As a consequence, the same oligomeric structure can be obtained by permutations of the various molecules. Moreover, when one considers several independent simulations, there is no reasonable criterion to define that a single molecule in one trajectory corresponds to another molecule in a different simulation. Even in a single-multimolecule simulation, one must correctly treat degenerate states, that is, those in which the same oligomer conformation is sampled by permutations of different molecules.

To describe the structure and dynamics of oligomers during peptide aggregation, in this article, we propose a new method that correctly accounts for the degeneracy of the multimolecule system. The approach is based on the recently proposed “by-parts” strategy,³⁴ which partitions a complex molecular system into parts, determines the metastable conformational states of each part, and describes the overall conformational state of the system in terms of a product basis of the states of the parts. Employing $(A\beta_{16-22})_3$ as a simple but instructive example, the method consists of three steps: (i) characterization of the *intramolecular* structure, that is, of the conformational states of a single $A\beta_{16-22}$ molecule in the presence of the other molecules (e.g., β -strand or random coil); (ii) characterization of the *intermolecular* structure through the identification of all occurring aggregate states of the peptides (e.g., dimers or trimers); and (iii) finally, description of the *overall* conformational states of the system in terms of a product basis of the three “single-molecule” states and the aggregate states. Based on these overall conformational states, one can construct a network^{35,36} reflecting the free energy landscape of the aggregation process and identify the aggregation pathways of the system.

2. METHODS

2.1. MD Simulation Setup. We used the MD data of Nguyen et al.²⁹ in our analysis of $(A\beta_{16-22})_3$. Starting from various configurations at peptide concentration of 65 mM with the three monomers far apart from each other and in random-coil conformation, they ran five MD trajectories of $\sim 1.4\text{-}\mu\text{s}$ total length. All simulations employed the GROMACS program suite,³⁷ combined with the GROMOS96 force field 43a1 of ref 38 to model the peptides and the simple-point-charge model³⁹ to explicitly account for the water solvent. During the simulations, the temperature was kept constant at 300 K. Snapshots of the trajectories were taken every 2 ps for analysis. For further details, see ref 29.

2.2. Principal Component Analysis. To reduce the dimensionality of the high-dimensional MD data, we employed a principal component analysis^{40,41} of the backbone dihedral angles (dPCA).⁴² Avoiding artifacts due to the mixing of overall and internal motion, dPCA has proven valuable for the conformational analysis of highly flexible molecules. The method is based on the covariance matrix $\sigma_{ij} = \langle (q_i - \langle q_i \rangle)(q_j - \langle q_j \rangle) \rangle$, where q_1, \dots, q_{2N} are the sine- and cosine-transformed φ and ψ dihedral angles of the peptide backbone and $\langle \dots \rangle$ denotes the average over all sampled conformations. By diagonalizing σ , we obtain $2N$ eigenvectors $\mathbf{v}^{(i)}$ and eigenvalues λ_i that are rank-ordered such that λ_1 represents the largest eigenvalue. The principal components $V_i = \mathbf{v}^{(i)} \cdot \mathbf{q}$ of the data $\mathbf{q} = (q_1, \dots, q_{2N})^T$ can then be used, for example, to represent the free energy surface of the system $\Delta G(V) = -k_B T [\ln P(V) -$

P_{\max}]. Here, P is the probability distribution of the molecular system along the principal components V_i and P_{\max} denotes its maximum, which is subtracted to ensure that $\Delta G = 0$ for the lowest free energy minimum. In the case of $A\beta_{16-22}$, we considered the inner 12 ϕ and ψ backbone dihedral angles, resulting in 24 principal components after the sine/cosine transformation. Only the first three components showed a non-Gaussian distribution; they yielded about 40% of the total fluctuations.

2.3. Geometric Clustering. To identify and illustrate geometric clusters of the free energy landscape of the peptide, we used the Hartigan–Wong k -means algorithm⁴³ as implemented in the R program suite.⁴⁴ As input data, the first three principal components with a non-Gaussian distribution were used. As discussed in ref 45, this procedure yields the correct numbers of minima and barriers of the free energy landscape, while being much faster than performing clustering on the complete data set. As k -means clustering is sensitive to the initial conditions, the algorithm was run 400 times, and the best result was chosen.⁴⁵ To determine the optimal value of the cluster number $k = 10$, we maximized the index of Krzanowski and Lai⁴⁶ and performed a visual inspection of the partitioning.

2.4. Characterization of Secondary Structure. We monitored the secondary-structure composition of the peptide using the “broad” definition given in ref 24, which appeared to be better suited for flexible peptides in small oligomers than the standard DSSP algorithm.⁴⁷ By considering the ϕ and ψ dihedral angles of the peptide backbone, a β -strand state is confined to the polygon with the vertices $(-180, 180)$, $(-180, 126)$, $(-162, 126)$, $(-162, 108)$, $(-144, 108)$, $(-144, 90)$, $(-50, 90)$, $(-50, 180)$ on the Ramachandran plot, and the α -helix state is confined to the polygon $(-90, 0)$, $(-90, -54)$, $(-72, -54)$, $(-72, -72)$, $(-36, -72)$, $(-36, -18)$, $(-54, -18)$, $(-54, 0)$. All other regions are considered as coil. The peptide is in the β -strand (α -helix) conformation if at least any two consecutive residues are in the corresponding β -strand (α -helix) states and no two consecutive residues are in α -helix (β -strand) states. In all other cases, the peptide is classified as random coil.

2.5. Characterization of Aggregate States. Peptides that share at least one intermolecular hydrogen bond were considered to be in the same aggregate.¹⁸ To account for the relative orientation of any two $A\beta_{16-22}$ peptides, we calculated the angle Θ between their two vectors connecting the C_α atoms of Lys₁₆ and Glu₂₂. Given by the scalar product of two normalized vectors, we have $0^\circ \leq \Theta \leq 180^\circ$. We associated the values $0^\circ \leq \Theta \leq 50^\circ$ with a parallel orientation ($\uparrow\uparrow$), $130^\circ \leq \Theta \leq 180^\circ$ with an antiparallel orientation ($\uparrow\downarrow$), and other values with a random orientation (R). Permuted combinations (e.g., $\uparrow\downarrow$, $\downarrow\downarrow$, $\downarrow\uparrow$, $\uparrow\uparrow$, and $\uparrow\downarrow\downarrow$) were regarded as a single state.

2.6. Calculation of the Transition Matrix. Using the definition of either the aggregate states (section 3.2) or the overall states (section 3.3) of $(A\beta_{16-22})_3$, we converted the 3N-dimensional MD trajectory into a one-dimensional time series $n(t)$ with n being the (aggregate or overall) state at time t . To study the kinetics of the oligomerization process in this state space, we calculated from $n(t)$ the associated row-normalized transition matrix $\{T_{mn}\}$, where T_{mn} represents the probability that state n changes to state m within a certain lag time τ . The diagonal elements T_{nn} give the metastability of a state n ; the overall transition probability out of the state is $1 - T_{nn}$. We choose $\tau = 2$ ps, but the qualitative aspects of $\{T_{mn}\}$ do not

change for increasing τ . As an illustration, we represented the transition matrix as a network,^{35,36} where the nodes are the considered states and the edges are the transitions between these states. The identification of the basins of the network of overall states was done by visualizing the time evolution of the MD trajectory along the network. Essentially the same results were obtained from a kinetic clustering method.^{48,49}

2.7. Analysis and Visualization. We used the programs Octave⁵⁰ and R⁴⁴ for data analysis, VMD⁵¹ for visualization of molecular structures, and Visone⁵² for network analysis.

3. RESULTS AND DISCUSSION

3.1. Intramolecular Structure: Single-Molecule States.

In a hetero-oligomer simulation, the individual molecules of the oligomer can be readily followed in time, as they are chemically and physically different entities. In the case of a homo-oligomer, on the other hand, each molecule is an exact copy of the others. Because the same oligomeric structure can be obtained by permutations of the various molecules, a degeneracy problem emerges. One way to overcome this problem is to classify each of the obtained snapshots independently and, in a second step, compare them and identify the degenerate states. Here, we follow an alternative approach that requires the conformational characterization of only a single molecule.

To explain the basic idea, we consider an MD simulation of the aggregation of n identical molecules, each containing M atoms. The n -molecule simulation can be decomposed into n simulations of the single molecule; that is, we convert the $n \times 3M$ -dimensional trajectory with, say, T snapshots into a $3M$ -dimensional trajectory with $n \times T$ snapshots. Note that the conformational space sampled by the peptide during aggregation is expected to be different than the space sampled by the peptide simulated alone, because the interactions occurring during aggregation move the equilibrium toward structures that are not necessarily stable for a single molecule.⁵³

In the following discussion, we use the trajectory of the trimer $(A\beta_{16-22})_3$ given by Nguyen et al.²⁹ and the above-described procedure to obtain a single-molecule trajectory of the aggregation process. By performing a dPCA of this trajectory (see section 2), we construct the free energy surface of a single $A\beta_{16-22}$ peptide along the relevant first three principal components; see Figure 2. The energy landscape is characterized by several minima that correspond to metastable conformational states of the molecule. A first visual inspection suggests about eight states; a quantitative analysis using k -

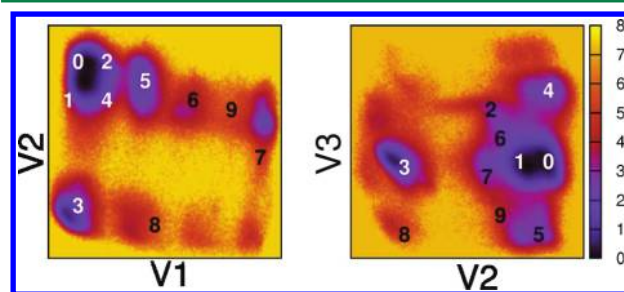


Figure 2. Free energy landscape (in units of $k_B T$) of a single $A\beta_{16-22}$ peptide obtained from an MD simulation of $(A\beta_{16-22})_3$, shown as a function of the principal components V_1 , V_2 , and V_3 . The numbers from 0 to 9 label the metastable conformational states of the system.

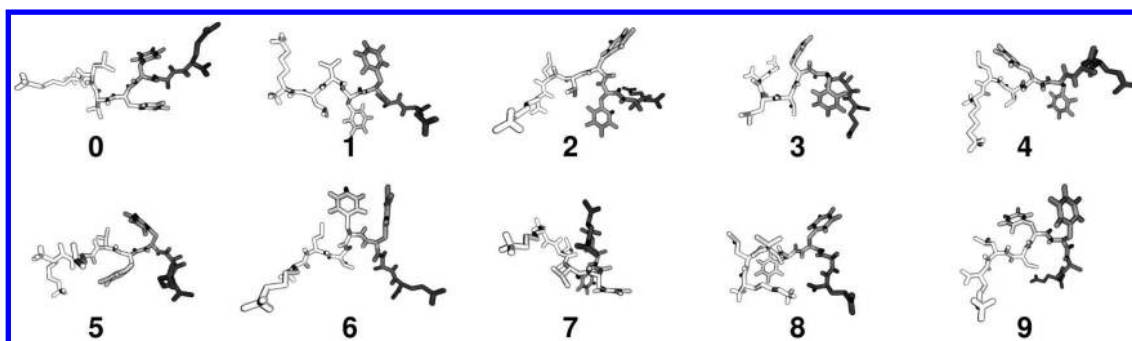


Figure 3. Representative molecular structures of the metastable conformational states of a single $A\beta_{16-22}$ peptide.

means clustering (see section 2) reveals the existence of 10 conformational states.

Figure 3 and Table 1 characterize the molecular structures of these states. They are labeled from 0 to 9 and ordered by

Table 1. Structural Characterization of the Single-Molecule States of $A\beta_{16-22}$, Labeled from 0 to 9, Including Populations P (in %) and Percentages of β -Sheet Conformation^a as Well as Probabilities (in %) of Various Aggregate States, Including Monomers (M), Dimers (D), Disordered Trimers (TD), and (Ordered) Trimers (T)⁵⁴

state	P	β	M	D	T^b	TD
0	22	98	0.9	9.3	55 (18)	35
1	21	98	0.4	7.8	60 (26)	32
2	17	96	0.7	3.0	42 (17)	55
3	14	94	0.6	2.1	72 (32)	25
4	7	73	0.6	2.4	59 (9)	38
5	7	71	0.7	1.4	22 (1)	76
6	6	64	2.8	3.3	67 (11)	27
7	5	27	43	0.8	37 (1)	19
8	2	21	8.6	2.6	66 (2)	23
9	1	56	5.7	3.5	22 (7)	69
average	—	87	3	5	54	38

^aRemaining structures are random coil. ^bPercentage to be the central molecule of the trimer in parentheses.

decreasing population. The first four states account for almost 75% of the full population. They lie in roughly the same region of the energy landscape in Figure 2, which corresponds to extended structures of the $A\beta_{16-22}$ peptide. Nonetheless, these

states exhibit different structural features (see Table SI and Figure S2, Supporting Information). States 4–9 show a considerable propensity to be in a random coil rather than to form a β -sheet (Table 1). The α -helix is rarely ($\leq 1\%$) sampled and is present only in clusters 7–9. State 8 corresponds to the starting conformation of the $A\beta_{16-22}$ peptides in the simulations. To ensure unbiased initial conditions, this structure was located far from the extended conformation necessary to form a β -sheet. It is noteworthy that the above results are different from the conformational distribution obtained from single-molecule MD simulations of $A\beta_{16-22}$, which yielded 62% random coil, 0.3% α -helix, and 38% β -sheet.^{24,29} These values change to 12%, 0%, and 87%, respectively, for three interacting $A\beta_{16-22}$ peptide.

The preceding analysis indicates that the conformation of each $A\beta_{16-22}$ peptide can switch between the 10 states shown in Figure 3. It is important to recall that these states occur not in a simulation of an isolated peptide but in a multimolecule simulation, during which the three molecules interact and aggregate with each other. Hence, it is interesting to correlate the above-defined single-molecule states with the preferred aggregate states of the system. To this end, Table 1 shows the probability that a given single-molecule state occurs in a certain aggregate state. Because $A\beta_{16-22}$ has a high propensity toward aggregation,²¹ we found about 3% as monomers (M), 5% as dimers (D), 54% as (ordered) trimers (T), and 38% as disordered trimers (TD).⁵⁴ In TD aggregates, all three $A\beta_{16-22}$ peptides are in contact with each other, whereas in a normally ordered trimer, only the central peptide makes contact with the other two, thus forming a layer. In the latter case, we also

Table 2. Structural Characterization of the Aggregate States of $(A\beta_{16-22})_3$,^a Including the Probability (in %) of the Single-Molecule Composition of Each Aggregate State^b and the Overall Population (in %) of Each Aggregate State

state	M	DR	$D\uparrow\uparrow$	$D\uparrow\downarrow$	TD	TR	$T\uparrow\uparrow$	$T\uparrow\uparrow\downarrow$	$T\uparrow\downarrow$	$T\uparrow\downarrow\uparrow$
0	7	16	8	32	20	22	24	5	23	27
1	5	10	12	24	17	16	15	4	20	32
2	7	14	9	7	24	25	12	3	14	13
3	10	10	2	4	9	4	4	61	21	10
4	5	5	5	2	7	6	13	25	3	6
5	6	5	15	1	13	9	4	1	5	1
6	12	21	17	1	4	9	17	1	5	9
7	19	12	12	28	2	5	11	0	7	1
8	19	5	18	1	1	1	0	0	2	2
9	9	3	2	1	2	3	0	0	1	0
overall	0.4	0.8	0.2	6.6	38	5.7	0.1	6.8	15	26.1

^aSee text for definition. ^bThis is the column normalized version of Table SII (Supporting Information), which lists the number of occurrences a certain single-molecule conformation is in a certain aggregate state.

determined the probability that the molecule is at one of the two outer sides of the trimer. We note that only the first few states have a large propensity to be in the central part of an ordered trimer. Being almost completely in β conformation, these states are able to make hydrogen bonds on both sides to build up a β -sheet layer.

3.2. Intermolecular Structure: Aggregate States. Using the definitions given in section 2, the multimolecule MD trajectory was analyzed to reveal the numbers and kinds of oligomers for every MD frame and to characterize the relative orientation of the molecules in each of the oligomers. In the case of $(A\beta_{16-22})_3$, either three monomers (M), one monomer and one dimer (D), or one trimer (T) was sampled. The dimers can be parallel ($D\uparrow\uparrow$), antiparallel ($D\uparrow\downarrow$), or in a random (DR) orientation. As mentioned above, the trimer can be disordered (TD, i.e., all three molecules are in contact with each other) or ordered (i.e., only the central molecule is in contact with the other two). The ordered trimer can be further described as follows:

- TR, all three molecules are in random orientation (5.7%);
- $T\uparrow\downarrow$, two antiparallel and the third random (15%);
- $T\uparrow\uparrow$, two parallel and the third random (0.1%);
- $T\uparrow\uparrow\downarrow$, two parallel and the third antiparallel (6.8%);
- $T\uparrow\downarrow\downarrow$, all antiparallel (26%); or
- $T\uparrow\uparrow\uparrow$, all parallel (0%).

The most populated configurations are the disordered trimer TD (38%) and the antiparallel β -sheet $T\uparrow\downarrow\downarrow$ (26%). Interestingly, the parallel-sheet $T\uparrow\uparrow\uparrow$ is not populated at all, which is in line with the fact that $A\beta_{16-22}$ oligomers are known to prefer antiparallel configurations.²¹ To correlate the aggregate states with the above-defined single-molecule states, Table 2 shows the structural characterization of the aggregate states in terms of the 10 single-molecule states. (For clarity, see ref 54.) Moreover, Table SII (Supporting Information) lists the number of structures simultaneously found in a certain single-molecule state and a certain aggregate state. The general trend is that longer aggregates, that is, the trimers, are populated by peptides belonging to the more populated clusters. The reason is that such peptides assume extended conformations and are therefore more suitable to be involved in the elongation of the oligomer. The low-populated clusters are mainly involved in M or DR and $D\uparrow\uparrow$.

To illustrate the possible transitions between the various aggregate states, we calculated the corresponding transition matrix $\{T_{mn}\}$ of $(A\beta_{16-22})_3$ (Table SIII, Supporting Information; for the definition, see section 2). Disregarding for clarity the low-populated states [M (0.4%), DR (0.8%), $D\uparrow\uparrow$ (0.2%), and $T\uparrow\uparrow$ (0.1%)], Figure 4 shows a network representation of the transition matrix. Of the dimers, $D\uparrow\downarrow$ is the most populated (7%) and also the most stable, with a metastability of 0.87 (see section 2). That is, the antiparallel orientation is preferred already at the dimer level. Of the trimers, the most prominent states are $T\uparrow\downarrow\downarrow$, which represents the proper antiparallel β -sheet with high metastability (0.96), and the even higher-populated (38%) disordered trimer state TD, with a metastability of 0.88. Coming from $D\uparrow\downarrow$, the system can go either directly to $T\uparrow\downarrow\downarrow$, or—more likely—first to $T\uparrow\downarrow$. Hence $T\uparrow\downarrow$ is the preferred target state for transitions from the dimers. On the trimer level, it turns out to be difficult to assign clear or prominent pathways. As shown below, this reflects the fact that the aggregate states are energetically and structurally not well-

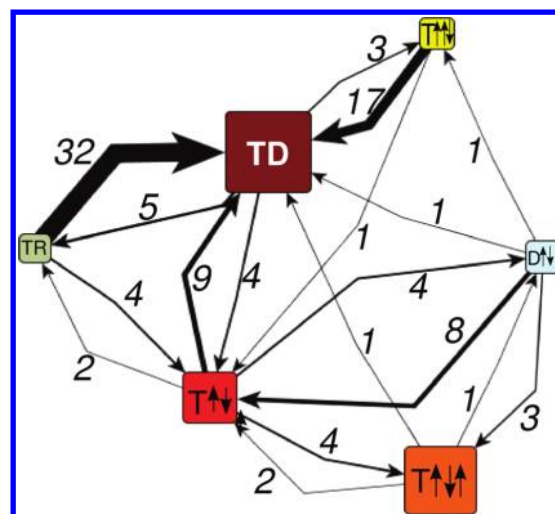


Figure 4. Transition network of the aggregate states of $(A\beta_{16-22})_3$. The areas of the nodes reflect their populations; the width of the arrows and the numbers refer to their transition probabilities (in percentages). Nodes shown include the dimer $D\uparrow\downarrow$ (antiparallel) and the trimers TR (random), TD (disordered), $T\uparrow\downarrow$ (two antiparallel and the third random), $T\uparrow\uparrow\downarrow$, and $T\uparrow\downarrow\uparrow$. The color code is in line with that in Figures 5 and 7.

defined. Without further characterization, these states are therefore not well-suited to represent the energy landscape and the kinetics of the aggregation process.

3.3. Overall Conformational States. Having introduced the single-molecule states (for the intramolecular structure) and the aggregate states (for the intermolecular structure) of $(A\beta_{16-22})_3$, we now combine this information to obtain a comprehensive characterization of the structure of the system. We first consider the intramolecular degrees of freedom represented by the 10 single-molecule states. To describe the intramolecular structure of the three molecules of $(A\beta_{16-22})_3$, we construct a product basis from the single-molecule states, which contains $10 \times 10 \times 10$ possible combination states. Of these, only 593 are sampled during the simulation. However, this value is still an overestimation, as some combinations are degenerate. For example, trimers with peptides in state combinations 5–4–4, 4–4–5, and 4–5–4 represent the same state, as they are permutations of the same configuration. After removing this degeneracy, we obtain 214 unique combinations. Of these, only 25 are necessary to cover 70% of the full trajectory (Figure S2, Supporting Information).

Finally, we define the overall conformational states of the trimer, given in the product basis of the 214 intramolecular state combinations and the 10 aggregate states of the system. Of these 2140 states, only 1255 are sampled by the trajectory. This number can be further reduced by considering the metastability of these states. Through the construction of the product basis, we obtain a large number (540) of very short-lived states, most of which are accessed for only a single MD snapshot. Accounting for structural fluctuations rather than for conformational transitions, these states can be safely discarded. Moreover, we choose to neglect states with $\Delta G \geq 7.8k_B T$, where $\Delta G \propto -k_B T \ln P$ and P is the population. This leaves us with 696 overall conformational states of $(A\beta_{16-22})_3$, representing 99.6% of the total population.

3.4. Free Energy Landscape of Peptide Aggregation. Employing the above-defined overall conformational states of $(A\beta_{16-22})_3$, we are now in a position to construct various

representations of the free energy landscape of $(A\beta_{16-22})_3$ and to discuss the kinetics of the oligomerization process. To characterize the free energy and the stability of the overall states, Figure 5 shows the statistical distribution of these

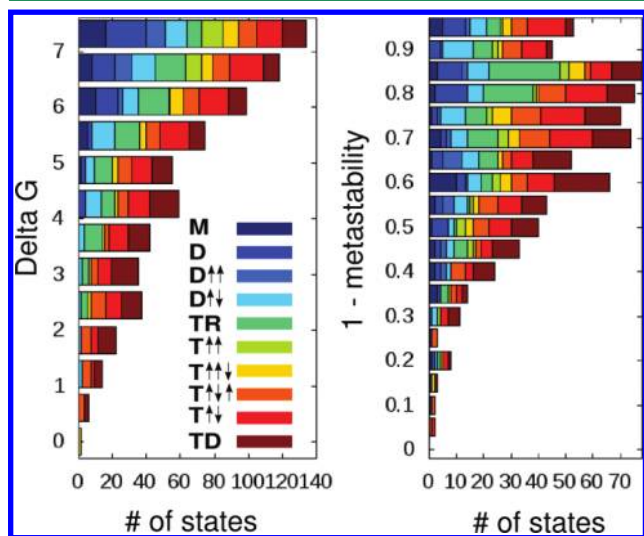


Figure 5. Histograms of (left) the free energy (in units of $k_B T$) and (right) the overall transition probabilities (i.e., $1 - \text{metastability}$) of the overall conformational states of $(A\beta_{16-22})_3$. The color code reflects the aggregate state. Note the overall funnel shape of the chosen representation of the data.

quantities. The resulting representation of the free energy landscape reveals numerous low-populated states (high ΔG) and a few highly populated states (low ΔG), which leads to an overall funnel shape of the data. A similar picture is provided by the histogram of the overall transition probabilities (i.e., $1 - \text{metastability}$; see section 2), which shows numerous relatively unstable and few highly stable overall states. To correlate the two properties, Figure 6 shows a graphical representation of the corresponding transition matrix (see section 2), where the states are ordered by decreasing population. We found that the upper triangle of the matrix is significantly more populated than

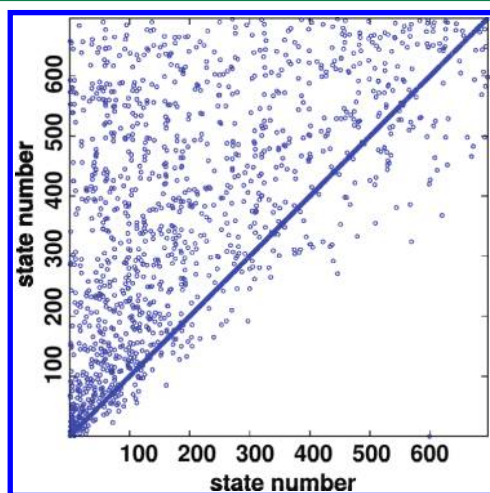


Figure 6. Graphical representation of the transition matrix associated with the overall conformational states of $(A\beta_{16-22})_3$. The states are ordered by decreasing population; only transitions with a probability of ≥ 0.1 are included.

the lower. This means that most transitions are directed to higher-populated states and that transitions to lower-populated states are unlikely. In other words, the transition network of the overall states fulfills detailed balance. Similar results were obtained when the transition matrix was ordered by decreasing metastability (Figure S3, Supporting Information). Transforming the populations to free energies through $\Delta G \propto -k_B T \ln P$, this finding again supports the funnel picture of the free energy landscape in which numerous high-energy states of low metastability preferably convert into a few metastable states of low energy. Whereas a free energy funnel can be expected,^{32,53} we note that, through the introduction of the overall states, we are in a position to actually calculate and characterize the energy landscape of aggregation from an MD simulation.

Using a color-coded histogram representation, Figure 5 decomposes the energy and stability distributions of the overall states in terms of their aggregate states. As expected, the overall states that reflect monomers (M) and dimers (D) have, on average, a higher energy than trimer overall states. Surprisingly, however, the free energy and the stability of the overall states depends only slightly on its aggregate state. Trimers, for example, are found not only at low energy but in the entire displayed energy range. Because the energetics and the stability of states are crucial for their dynamics, these findings explain why aggregate states alone are not a good description of the aggregation process (Figure 4).

To illustrate the energy landscape and the pathways of the oligomerization process, Figure 7 displays a network representation of the transition matrix, where the nodes are the overall states of $(A\beta_{16-22})_3$ and the edges are the transitions among them.^{35,36,55} Arranging the nodes such that the overlap of the links is minimized, the network can be partitioned into five sections, I–V, corresponding to basins of the free energy landscape (see section 2). Qualitatively speaking, all trajectories start as three monomers in basin I and pass the intermediate basins II–IV before they end up in basin V, containing the final states of the aggregation process, most notably the all-antiparallel trimer. Table 3 lists various properties of the basins, including their population P , their number of states n , their average connectivity k , and their content of the various aggregate states. Interestingly, we found that all energy basins contain mixtures of different aggregate states. This explains why the aggregate states alone are not a good descriptor of the dynamics; see Figure 4. Moreover, we found that the connectivity k (average number of directed edges per state) differs significantly, ranging from $k = 2$ for basin I to $k = 13$ for basin III. As shown in Figure S4 (Supporting Information), the values of the connectivity can depend sensitively on the definition of the edges; for example, one considers only transitions that happen at least x times. By changing this threshold, we learned that a large value for the connectivity can be caused by highly frequented transitions (basin V) or by a large number of possible transitions (basin III). The 200 states with largest k values are indicated by triangular nodes in Figure 7.

Analyzing the network, we can identify the main aggregation pathways of $(A\beta_{16-22})_3$. By construction, all trajectories start with three monomers in the single-molecule state (888). This initial state is located in basin I, which is the least populated basin (0.3%) and contains only short-lived monomer and dimer states. Basin V, on the other hand, comprises the end states of the aggregation process, most notably the all-antiparallel state

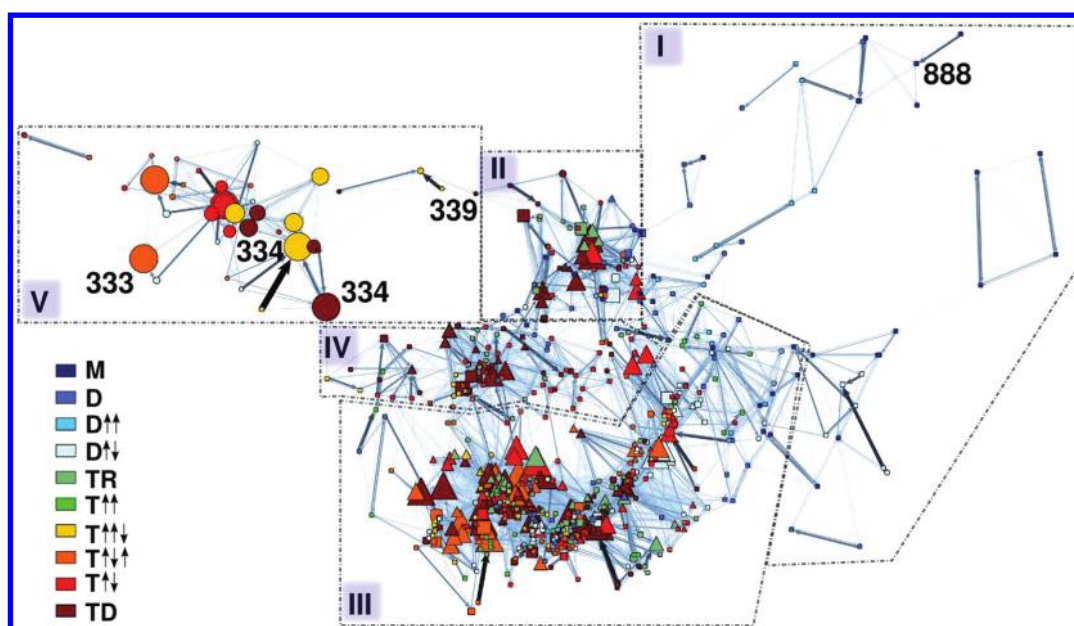


Figure 7. Transition network constructed from the overall states of $(A\beta_{16-22})_3$, reflecting the energy landscape and the pathways of the oligomerization process of the peptide. The areas of the nodes reflect their population, the widths of the arrows account for the associated transition probabilities, and the color code reflects the aggregate state. A circular-shaped node identifies states with at least two peptide belonging to cluster 3. The triangular shape discriminates the 200 states with highest connectivity (k). Three-digit numbers denote the single-molecule states of a few important overall states, such as the starting state (888) and the all-antiparallel end state (333). Dashed lines indicate the borders of energy basins I–V of the free energy landscape.

Table 3. Characterization of the Basins of the Free Energy Landscape in Figure 7, Showing the Population P (in %), the Number of States n , the Average Connectivity k , and the Content of the Various Aggregate States (in %) of Each Basin

	P	n	k	M	DR	D↑↑	D↑↓	TR	T↑↑	T↑↑↓	T↑↑↑	T↑↓	TD
I	0.3	51	2.1	45	25	18	12						
II	7	71	10.3	13	13	3	7	17		1	3	18	25
III	74	434	13.0	2	8	3	13	17	5	6	15	17	17
IV	4	101	4.7	1	5			13	2	6	7	32	35
V	15	39	8.2				15			18	26	23	18

(333). Although providing only 6% of the total number of states, this basin holds about 15% of the total population. It contains mostly trimer and some $D\uparrow\downarrow$ states; that is, the $\uparrow\downarrow$ core is maintained. Correspondingly, basin V contains mainly single-molecule states of the type (33x), which are indicated by round nodes in Figure 7.

Next, we identified the connections of basins I and V to their neighboring basins. Interestingly, we note that basin V is almost exclusively connected to basin IV (apart from a very few transitions to basin II). The $IV \leftrightarrow V$ transitions occur through the state (334)TD, which represents a gateway between the two basins. Basin IV contains about 100 relatively short-lived trimer states with an overall population of 4%. Coming from basin I, on the other hand, basin II is the most likely connection. Similarly to I, this basin contains numerous monomers and dimers, as well as mostly random and disordered trimers. Unlike basin I, this basin is significantly populated (7%) and holds relatively long-lived states.

Given the start in basin I and the end in basin V, the various aggregation pathways mainly differ in the way the three intermediate basins are visited. Here, the main hub is intermediate basin III; $(A\beta_{16-22})_3$ spends over 70% of the simulation time in this region. It contains more than 400 states, which can adopt all possible aggregate states. Basin III also exhibits the highest connectivity k of all basins (Table 3).

Taking these results together, we conclude that basin III is a typical example of a kinetic trap that comprises numerous misfolded conformations. Although the conformational transitions between the basins occur within picoseconds, the systems spends a considerable time in these misfolded intermediate states. As was found in folding simulations,⁵⁶ kinetic traps can significantly affect the overall time scale of the aggregation process.

4. CONCLUSIONS

To describe the structural dynamics of peptide aggregation, we have outlined a new method that allows for the identification and characterization of the different molecular structures occurring during the process. The approach is general, as no a priori knowledge of the dynamics of the process or the structure of the encounter complex is required. This is important because the internal structure of the fibrils seems to depend on the fibril growth conditions.⁷ Moreover, the approach considers both the intramolecular and intermolecular structures and correctly accounts for the degeneracy of the multimolecule system. The method consists of three steps and involves three types of conformational states that should be carefully distinguished: (i) The *intramolecular* structure of each individual molecule is described in terms of *single-molecule* states, which can be obtained through a dPCA of the single-

molecule trajectory followed by some clustering (section 3.1). In the case of $(A\beta_{16-22})_3$, we identified 10 single-molecule states that account for the conformational preferences (e.g., to be in a β -strand or a random coil) of a single $A\beta_{16-22}$ molecule in the presence of the other molecules. (ii) The *intermolecular* structure is described in terms of the *aggregate states* of the peptides, which can be directly obtained from an analysis of the multimolecule trajectory (section 3.2). In the case of $(A\beta_{16-22})_3$, we found, for example, dimers or trimers in parallel or antiparallel orientation. (iii) Applying the recently suggested by-parts strategy,³⁴ the *overall* conformational states of the system are given in terms of a product basis of the single-molecule states of each $A\beta_{16-22}$ molecule and the aggregate states (section 3.3). It should be noted that only a few of the (in principle exponentially many) overall states are populated in the aggregation process. For example, we obtained ~ 700 overall states in the case of $(A\beta_{16-22})_3$.

The analysis of the overall conformational states allows a picture to be drawn of the free energy landscape of the aggregation process. For example, the statistical distribution of the free energy and the stabilities of these states (Figures 5 and 6) revealed an overall funnel shape of the energy landscape in which numerous high-energy states of low metastability preferably convert into a few metastable states of low energy. Interestingly, we found that the free energy and stability of the overall states depends only slightly on its aggregate state. Because the energetics and the stability of states are crucial for the their dynamics, these findings explain why aggregate states alone are not a good description of the aggregation process (Figure 4).

By constructing a transition network from the overall states, we found that the network can be partitioned in five parts corresponding to basins of the free energy landscape. This representation facilitates the description of the aggregation pathways of $(A\beta_{16-22})_3$. By construction, all trajectories start with three monomers in basin I, which is the least populated basin and contains only short-lived monomer and dimer states. Proceeding through some combination of the intermediate basins II–IV, the system ends up in basin V, which contains the final states of the aggregation process, most notably the all-antiparallel trimer. A global picture of the oligomerization therefore consists of three phases. In the short (approximately nanosecond) initial phase, the individual $A\beta_{16-22}$ peptides convert from a monomeric form to some disordered dimer or trimer (basins I and II). In the subsequent intermediate phase (basins III and IV), the overall states rapidly interconvert among themselves, not allowing the oligomer to reach its optimum conformation. In particular, basin III acts as a kinetic trap and considerably increases the overall time scale of the aggregation process. To reach basin V, the system needs to pass a gateway from basin IV through the state (334)TD. This happens in the final phase, where a hydrophobic collapse of the $(A\beta_{16-22})_3$ into a disordered trimer state occurs. During this event, the single molecules rearrange into the appropriate (33x) single-molecule conformations, which seems to be necessary to access basin V.

The generalization of the method to analyze the aggregation of an n -mer is, at least in principle, straightforward. In step i, the single-molecule trajectory is readily generated as described above; that is, the computational effort does not depend on n . In step ii, the construction of the aggregate states depends on the properties of the considered system, such as the length of the monomers. For example, one could consider the

intermolecular distance between specific residues and take into account whether the interactions are native. Moreover, the number of aggregate states could strongly increase with the system size n . The facts that no all-parallel trimer was found for $(A\beta_{16-22})_3$ and that a stepwise growth of the oligomer is typically observed in MD simulations,^{18,29} however, suggest that, in practice, the number of aggregate states should grow linearly in the course of the assembly. The construction of the overall states in step iii is again a simple matter. With increasing system size, it becomes important to regard the overall states as “microstates” and perform a kinetic clustering in this basis, which yields the main basins of the energy landscape. Finally, we note that the present analysis can be readily applied to a coarse-grained simulation, which enables an enhanced sampling of the aggregation process.

■ ASSOCIATED CONTENT

Supporting Information

Mean values (Table SI) and distributions (Figure S1) of the dihedral angles of the single-molecule states, total number of structures found in a certain single-molecule state (Table SII), transition matrix of the aggregate states (Table SIII), convergence of the combinations of single conformational states (Figure S2), transition matrix of the overall states sorted by their metastability (Figure S3), and the normalized degree of the five basins (Figure S4). This material is available free of charge via the Internet at <http://pubs.acs.org>.

■ AUTHOR INFORMATION

Corresponding Author

*E-mail: stock@physik.uni-freiburg.de.

Notes

The authors declare no competing financial interest.

■ ACKNOWLEDGMENTS

We thank Abhinav Jain and Francesco Rao for numerous inspiring and helpful discussions.

■ REFERENCES

- (1) Dobson, C. M. *Trends Biochem. Sci.* **1999**, *24*, 329–332.
- (2) Selkoe, D. J. *Nature (London)* **2003**, *426*, 900–904.
- (3) Booth, D. R.; Sunde, M.; Bellotti, V.; Robinson, C. V.; Hutchinson, W. L.; Fraser, P. E.; Hawkins, P. N.; Dobson, C. M.; Radford, S. E.; Blake, C. C. F.; Pepys, M. B. *Nature (London)* **1997**, *385*, 787–793.
- (4) Chiti, F.; Dobson, C. M. *Annu. Rev. Biochem.* **2006**, *75*, 333–366.
- (5) Makin, O. S.; Serpell, L. C. *FEBS J.* **2005**, *272*, 5950–5961.
- (6) Chiti, F.; Webster, P.; Taddei, N.; Clark, A.; Stefani, M.; Ramponi, G.; Dobson, C. M. *Proc. Natl. Acad. Sci. U.S.A.* **1999**, *96*, 3590–3594.
- (7) Petkova, A. T.; Leapman, R. D.; Guo, Z.; Yau, W.-M.; Mattson, M. P.; Tycko, R. *Science* **2005**, *307*, 262–265.
- (8) Lee, J.; Culyba, E. K.; Powers, E. T.; Kelly, J. W. *Nat. Chem. Biol.* **2011**, *7*, 1–8.
- (9) Cecchini, M.; Rao, F.; Seeber, M.; Cafisch, A. *J. Chem. Phys.* **2004**, *121*, 10748.
- (10) Tarus, B.; Straub, J. E.; Thirumalai, D. *J. Am. Chem. Soc.* **2006**, *128*, 16159–16168.
- (11) Tsemekhman, K.; Goldschmidt, L.; Eisenberg, D.; Baker, D. *Protein Sci.* **2007**, *16*, 761–764.
- (12) Strodel, B.; Fitzpatrick, A. W.; Vendruscolo, M.; Dobson, C. M.; Wales, D. J. *J. Phys. Chem. B* **2008**, *112*, 9998–10004.
- (13) Takeda, T.; Klimov, D. K. *Biophys. J.* **2009**, *96*, 442–452.

- (14) O'Brien, E. P.; Okamoto, Y.; Straub, J. E.; Brooks, B. R.; Thirumalai, D. *J. Phys. Chem. B* **2009**, *113*, 14421–14430.
- (15) Reddy, G.; Straub, J. E.; Thirumalai, D. *Proc. Natl. Acad. Sci. U.S.A.* **2009**, *106*, 11948–11953.
- (16) Vitalis, A.; Caflisch, A. *J. Mol. Biol.* **2010**, *403*, 148–165.
- (17) Rojas, A.; Liwo, A.; Browne, D.; Scheraga, H. A. *J. Mol. Biol.* **2010**, *404*, 537–552.
- (18) Matthes, D.; Gapsys, V.; Daebel, V.; de Groot, B. L. *PloS One* **2011**, *6*, e19129.
- (19) Straub, J. E.; Thirumalai, D. *Annu. Rev. Phys. Chem.* **2011**, *62*, 437–463.
- (20) Tarus, B.; Straub, J. E.; Thirumalai, D. *J. Mol. Biol.* **2008**, *379*, 815–829.
- (21) Balbach, J. J.; Ishii, Y.; Antzutkin, O. N.; Leapman, R. D.; Rizzo, N. W.; Dyda, F.; Reed, J.; Tycko, R. *Biochemistry* **2000**, *39*, 13748–13759.
- (22) Favrin, G.; Irbäck, A.; Mohanty, S. *Biophys. J.* **2004**, *87*, 3657–3664.
- (23) Ma, B.; Nussinov, R. *Proc. Natl. Acad. Sci. U.S.A.* **2002**, *99*, 14126–14131.
- (24) Klimov, D. K.; Thirumalai, D. *Structure (London)* **2003**, *11*, 295–307.
- (25) Röhrig, U. F.; Laio, A.; Tantalo, N.; Parrinello, M.; Petronzio, R. *Biophys. J.* **2006**, *91*, 3217–3229.
- (26) Gnanakaran, S.; Nussinov, R.; Garca, A. E. *J. Am. Chem. Soc.* **2006**, *128*, 2158–2159.
- (27) Takeda, T.; Klimov, D. K. *J. Mol. Biol.* **2007**, *368*, 1202–1213.
- (28) Fawzi, N. L.; Okabe, Y.; Yap, E.-H.; Head-Gordon, T. *J. Mol. Biol.* **2007**, *365*, 535–550.
- (29) Nguyen, P. H.; Li, M. S.; Stock, G.; Straub, J. E.; Thirumalai, D. *Proc. Natl. Acad. Sci. U.S.A.* **2007**, *104*, 111–116.
- (30) Nguyen, P. H.; Li, M. S.; Derreumaux, P. *Phys. Chem. Chem. Phys.* **2011**, *13*, 9778–9788.
- (31) Tsai, H.-H. G.; Reches, M.; Tsai, C.-J.; Gunasekaran, K.; Gazit, E.; Nussinov, R. *Proc. Natl. Acad. Sci. U.S.A.* **2005**, *102*, 8174–8179.
- (32) Strodel, B.; Whittleston, C. S.; Wales, D. J. *J. Am. Chem. Soc.* **2007**, *129*, 16005–16014.
- (33) Stock, G.; Jain, A.; Riccardi, L.; Nguyen, P. H. In *Protein and Peptide Folding, Misfolding and Non-Folding*; Schweitzer-Stenner, R., Ed.; Wiley: New York, 2012; p 57.
- (34) Jain, A.; Hegger, R.; Stock, G. *J. Phys. Chem. Lett.* **2010**, *1*, 2769–2773.
- (35) Rao, F.; Caflisch, A. *J. Mol. Biol.* **2004**, *342*, 299–306.
- (36) Noe, F.; Horenko, I.; Schütte, C.; Smith, J. C. *J. Chem. Phys.* **2007**, *126*, 155102.
- (37) van der Spoel, D.; Lindahl, E.; Hess, B.; Groenhof, G.; Mark, A. E.; Berendsen, H. J. C. *J. Comput. Chem.* **2005**, *26*, 1701–1718.
- (38) van Gunsteren, W. F.; Billeter, S. R.; Eising, A. A.; Hünenberger, P. H.; Krüger, P.; Mark, A. E.; Scott, W. R. P.; Tironi, I. G. *Biomolecular Simulation: The GROMOS96 Manual and User Guide*; Vdf Hochschulverlag AG an der ETH Zürich: Zürich, Switzerland, 1996.
- (39) Berendsen, H. J. C.; Postma, J. P. M.; van Gunsteren, W. F.; Hermans, J. In *Intermolecular Forces*; Pullman, B., Ed.; D. Reidel Publishing Company: Dordrecht, The Netherlands, 1981; pp 331–342.
- (40) Amadei, A.; Linssen, A. B. M.; Berendsen, H. J. C. *Proteins* **1993**, *17*, 412–425.
- (41) de Groot, B. L.; Daura, X.; Mark, A. E.; Grubmüller, H. *J. Mol. Biol.* **2001**, *309*, 299–313.
- (42) Altis, A.; Nguyen, P. H.; Hegger, R.; Stock, G. *J. Chem. Phys.* **2007**, *126*, 244111.
- (43) Hartigan, J. A.; Wong, M. A. *Appl. Stat.* **1979**, *28*, 100–108.
- (44) R: A Language and Environment for Statistical Computing; R Foundation for Statistical Computing: Vienna, Austria, 2005.
- (45) Altis, A.; Otten, M.; Nguyen, P. H.; Hegger, R.; Stock, G. *J. Chem. Phys.* **2008**, *128*, 245102.
- (46) Krzanowski, W.; Lai, Y. *Biometrics* **1988**, *44*, 22–34.
- (47) Kabsch, W.; Sander, C. *Biopolymers* **1983**, *22*, 2577–2637.
- (48) Jain, A.; Stock, G., manuscript submitted.
- (49) Rao, F. *J. Phys. Chem. Lett.* **2010**, *1*, 1580–1583.
- (50) Eaton, J. W. *GNU Octave Manual*; Network Theory Limited: New York, 2002.
- (51) Humphrey, W.; Dalke, A.; Schulten, K. *J. Mol. Graph.* **1996**, *14*, 33–38.
- (52) Brandes, U.; Wagner, D. In *Graph Drawing Software*; Junger, M., Mutzel, P., Eds.; Springer-Verlag: New York, 2004; pp 321–340.
- (53) Clark, P. L. *Trends Biochem. Sci.* **2004**, *29*, 527–534.
- (54) To characterize the structure of the single-molecule states of $(A\beta_{16-22})_3$ in Table 1, we use the symbols *M* and *D* to indicate that the single molecule is in a monomer and a dimer state, respectively, independently of the remaining molecule(s). To characterize the structure of the aggregate states in Table 2, on the other hand, we use the symbols *M* and *D* to indicate that the system exists as three monomers and as one monomer and one dimer, respectively.
- (55) Gfeller, D.; De Los Rios, P.; Caflisch, A.; Rao, F. *Proc. Natl. Acad. Sci. U.S.A.* **2007**, *104*, 1817–1822.
- (56) Bowman, G. R.; Pande, V. S. *Proc. Natl. Acad. Sci. U.S.A.* **2010**, *107*, 10890–10895.